NEAR SOURCE ENERGY PARTITIONING FOR REGIONAL WAVES IN 2D AND 3D MODELS: CONTRIBUTIONS OF FREE SURFACE SCATTERING

Xiao-Bi Xie, Thorne Lay, Ru-Shan Wu, and Yaofeng He

University of California, Santa Cruz

Sponsored by Air Force Research Laboratory

Contract No. FA8718-05-C-0021

ABSTRACT

Regional seismic phases have become of central importance for low-yield nuclear event size estimation and discrimination. However, the lack of fundamental understanding of the physics controlling regional wave energy partitioning remains a major concern for high-confidence applications of regional phases in nuclear monitoring. Due to the complex excitation and energy partitioning processes involved in regional phase formation, it is difficult to separate the contributions of different excitation mechanisms in the observed data. Given this situation, numerical simulations can play an important role for understanding the excitation of regional phases.

We have developed a regional seismic wave numerical modeling method to investigate energy partitioning for explosion-generated signals. Our approach is to separate the problem into consideration of near-source energy partitioning effects apart from long-range propagation effects. This is achieved by combining the near source simulation, e.g., finite-difference modeling or boundary-element modeling, with a slowness analysis method. This method allows very fine near source models to be used to investigate the near-source energy partitioning process explicitly. A localized slowness analysis tracks the energy partitioning instead of a time consuming mode formation by long distance propagator. Recent empirical demonstrations that explosion generated shear waves have a corner frequency that scales approximately as $V_s(S)/R_e$ (Fisk, 2006), where R_e is the elastic radius and $V_s(S)$ is the source shear velocity, indicate the importance of very near-source processes for the energy partitioning. Our initial work has involved *P*-to-*S* energy conversion by near-source scattering, which intrinsically scales the *S* energy generation relative to the *P*-waves without systematically shifting the corner frequency of the explosion *S*-waves. We are now exploring mechanisms that may account for the corner frequency shift between *P* and *S* signals for explosions that preserve the yield scaling behavior. Scattering of *Rg*-to-*S* is one such mechanism, as *Rg* forms with a lower frequency content than *P.* The most effective mechanism for scattering of *Rg* is rough surface topography, although shallow crustal heterogeneity can be important too.

In this report, we apply a combined boundary element simulation and slowness analysis method to investigate the effect of near-source topographic scattering on the explosion source energy partitioning. Random free surface models with exponential power spectrum, variable rms fluctuations and correlation lengths are used in the calculation. In addition, we test the effects of intrinsic attenuation and source depth on the scattering process. The frequency dependence on different parameters is investigated. The results show that couplings caused by surface scattering do occur between the body and surface waves, and these processes influence the overall partitioning of the explosion energy. Additional trapped waveguide energy can be generated by the interaction between an explosion source and near-source topographic fluctuations. The source depth, rms value, correlation length and attenuation all affect this process.

OBJECTIVE

With the current emphasis on global monitoring for low-yield nuclear tests, regional seismic phases such as *Lg* have become very important for magnitude and yield estimation of underground nuclear tests (e.g. Nuttli, 1986; Patton, 2001). In addition, various *P*/*S*-type amplitude ratios for high frequency regional phases (e.g. *Pn*/*Sn*, *Pn*/*Lg*, *Pg*/*Lg*, *Pg*/*Sn*) have become important for event discrimination (e.g., Taylor et al., 1989; Kim et al., 1993, 1997; Walter et al., 1995; Fisk et al., 1996; Taylor, 1996; Taylor and Hartse, 1997; Hartse et al., 1997; Fan and Lay, 1998a–c; Xie, 2002; Bottone et al., 2002). The applications of regional phases for yield estimation and event discrimination are largely based on empirical approaches, and while very promising in many cases, there are major questions about the nature of excitation of *S*-wave dominated phases such as *Lg*. Numerous excitation processes have been proposed. The complex excitation and energy partitioning processes associated with regional phases make it difficult to empirically separate the contribution of individual energy partitioning mechanisms by data analysis. Numerical modeling approaches are thus of great importance for investigating the excitation and propagation of regional phases (e.g., Xie and Lay, 1994; Wu, et al., 2000a, b; Bonner et al., 2003; Stevens et al., 2003; Myers et al., 2003, 2005; Xie, et al., 2005a, b).

Although there are continuing controversies about the dominant *P*-to-*S* transfer mechanisms affecting regional phases, most investigators agree that appreciable energy from explosion sources is converted to *S*-waves in the near-source region. Fisk (2006) demonstrates that the *S*-wave excitation for explosions scales with explosion yield and has a corner frequency shift relative to *P* energy proportional to the source region velocity ratio *Vs(S)/Vp(S)*. Several possible near-source energy excitation mechanisms have been proposed to explain the generation of regional *Lg*-wave. Among these models, the near source coupling between *P*-, *S*- and the *Rg*-waves due to the scattering on a rugged free surface may play an important role for *Lg*-wave excitation. This has been investigated by different authors from both observational and theoretical perspectives. From data analysis, Gupta et al. (1992, 2005) suggested that near-source scattering of explosion-generated *Rg* into *S* makes a significant contribution to the low-frequency *Lg*. Patton and Taylor (1995) analyzed the *Lg* spectral ratios from Nevada Test Site (NTS) explosions and suggested that the *Lg*–wave is generated by near-source scattering of *Rg*-waves into body waves, which become trapped in the crust. Patton and Taylor (1995) and Gupta et al. (1997) introduced the theoretical model of spall source to explain the observed similarity between the *Rg* and *Lg* spectrum. McLaughlin and Jih (1988) used finite-difference simulation to investigate topography influences on teleseismic *P*-waveforms, and indicated possible *Rg*-to-*P* scattering due to the near source topography. Several more recent studies, e.g., Bonner et al. (2003), Myers et al. (2003), and Wu et al. (2003), also provided strong evidence in favor of the *Rg*-to-*S* scattering mechanism for the generation of the low frequency *S* and *Lg* for explosions. Myers et al. (2005), using numerical simulation, investigated the effect of topography on the *P*-to-*S* conversion. They concluded that near-source topography and geologic complexity in the upper crust strongly contribute to the generation of S-waves. Xie et al. (2005a, b) investigated the contribution of shallow scattering on the explosive source energy partitioning and calculated the frequency dependent *Lg* excitation functions. They found that the high-frequency *Lg* energy is from *P*-*pS*-to-*Lg* and *P*-to-*Lg* scattering, and the low-frequency energy comes from *Rg*-to-*Lg* scattering.

With the existence of a rugged free surface, the actual coupling between waves in the near source region is expected to be rather complex affecting the very formation of *Rg*, so it important to study this phenomenon with the source excitation in the model, not simply as a propagation effect. The scattering at the free surface can change the propagation direction of *pP*- and *pS*-waves causing some of their energy to become trapped in the crustal waveguide to contribute to the *Lg*-wave. A rugged free surface or shallow heterogeneity also provides coupling between the surface wave and body waves. Both body-wave to surface-wave and surface-wave to body-wave scattering could occur. Multiple scattering, source depth and attenuation in the shallow layers are all factors that may affect the result and should be considered in the investigation. Source depth, attenuation and statistical features of the surface fluctuation may add frequency dependency to the energy partitioning process. In this report, we use the 2D *P*-*SV* boundary-element simulation (Ge et al., 2005) and slowness analysis method (Xie et al., 2005a) to investigate the effect of topographic scattering on the explosion source energy partitioning. Topographic models with different rms fluctuations and correlation lengths are used in the numerical simulations, and their effects are examined.

RESEARCH ACCOMPLISHED

The Boundary Element Simulation

The boundary element method is formulated in terms of integrals along boundaries so that the traction-free condition on the free surface can be naturally treated. The method provides a geometrically accurate description of irregular boundaries. Among different numerical simulation methods such as the finite-difference method, the boundary integral method is more suitable for modeling complex reflections from the rugged topography. We use the 2D elastic boundary element method developed in the previous stage of this project (Ge et al., 2005) to simulate the effect of free surface scattering on the explosion source energy partitioning. The following is a brief description of the boundary element method.

Consider the layered crustal model shown in Figure 1. Each layer Ω has constant velocities and density but the free surface and the interfaces can be irregular. Γ_1 and Γ_2 are the free surface and the interface. Γ_∞ is the radiation boundary marked with dash lines. Based on the representation theorem (e.g., Aki and Richards, 1980), the wavefield within each layer can be expressed using the integral along its boundary (Ge et al., 2005)

$$\mathbf{C}(\mathbf{r})\mathbf{u}(\mathbf{r})+\int_\Gamma\left[\mathbf{u}(\mathbf{r}')\Sigma(\mathbf{r},\mathbf{r}')-\mathbf{t}(\mathbf{r}')\mathbf{G}(\mathbf{r},\mathbf{r}')\right]d\Gamma(\mathbf{r}')=\int_\Omega\mathbf{f}(\mathbf{r}',\omega)\mathbf{G}(\mathbf{r},\mathbf{r}')d\Omega(\mathbf{r}'), \tag{1}$$

where $\mathbf{u}(\mathbf{r})$ is the displacement, $\mathbf{r}$ is the position of observation point and $\mathbf{r}'$ is the scattering point, $\mathbf{t}(\mathbf{r}')$ is the traction vector on the boundary, the coefficient $\mathbf{C}(\mathbf{r})$ generally depends on the local geometry at $\mathbf{r}$, and $\mathbf{G}(\mathbf{r},\mathbf{r}')$ and $\mathbf{\Sigma}(\mathbf{r},\mathbf{r}')$ are the Green's functions for displacements and traction, respectively. $\mathbf{C}(\mathbf{r})$, $\mathbf{\Sigma}(\mathbf{r},\mathbf{r}')$ and $\mathbf{G}(\mathbf{r},\mathbf{r}')$ are all 2×2 matrices for a 2 D *P-SV* problems. $\mathbf{f}(\mathbf{r},\omega)$ is the body force distribution in the model. The green's functions $\mathbf{G}(\mathbf{r},\mathbf{r}')$ and $\mathbf{\Sigma}(\mathbf{r},\mathbf{r}')$ can be calculated using the elastic wave equation in unbounded homogeneous medium.

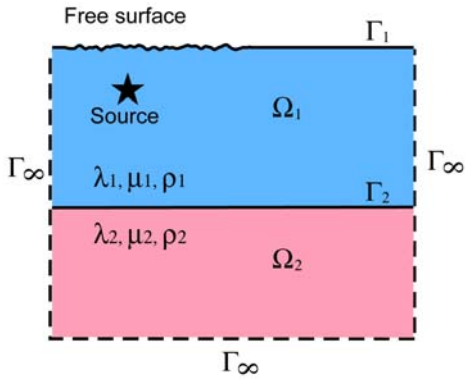

Figure 1. Geometry of a layered crustal model.

Taking the two-layer model as an example, using a delta distributed source $\mathbf{f}(\mathbf{r},\omega)=\mathbf{f}(\omega)\delta(\mathbf{r}_0)$, and considering the traction free boundary condition on the free surface and radiation boundary condition for Γ_∞, the equations for the first and second layers can be modified as (Ge et al., 2005)

$$\mathbf{C}(\mathbf{r})\mathbf{u}(\mathbf{r})+\int_{\Gamma_1}\Sigma(\mathbf{r},\mathbf{r}')\mathbf{u}(\mathbf{r}')d\mathbf{r}'+\int_{\Gamma_2}[\Sigma(\mathbf{r},\mathbf{r}')\mathbf{u}(\mathbf{r}')-\mathbf{G}(\mathbf{r},\mathbf{r}')\mathbf{t}(\mathbf{r}')]d\mathbf{r}'=\mathbf{G}(\mathbf{r},\mathbf{r}_0)\mathbf{f}(\omega) \tag{2}$$

and

$$\mathbf{C}(\mathbf{r})\mathbf{u}(\mathbf{r})+\int_{\Gamma_2}[\Sigma(\mathbf{r},\mathbf{r}')\mathbf{u}(\mathbf{r}')-\mathbf{G}(\mathbf{r},\mathbf{r}')\mathbf{t}(\mathbf{r}')]d\mathbf{r}'=0 \tag{3}$$

Equations (2) and (3) simultaneously provide the basis for calculating the wave propagation in a model with rugged free surface. The displacement $\mathbf{u}(\mathbf{r})$ on both Γ_1 and Γ_2 can be discretized and solved from these equations. Finally, the internal displacement field can be calculated from their boundary values using Equation (1).

Investigating the Boundary Scattering Using the Slowness Analysis Method

We use the slowness analysis method (Xie et al., 2005a) developed in this project to analyze the wavefield generated from the boundary element calculation and investigate the near source energy partitioning with the presence of free surface fluctuations. Figure 2 shows the configurations of calculations. In this simple example, we use two-layer models with different free surface parameters and source depths for boundary element calculations. The velocities and densities are listed in Table 1. The topographic fluctuation has an exponential power spectrum and a correlation length of 0.5 km. The fluctuations are located above the source and extend in both directions for 20 km. Illustrated in Figure 2(a) is the model with 150 m rms fluctuation (maximum peak to trough is 625 m), and in Figure 2(b) is the model with 300 m rms fluctuation (maximum peak to trough is 1,281 m). The source depths used in these calculations are 500 m and 3,000 m, respectively. The synthetic seismograms are generated in a vertical array of 41×60 receivers located between epicentral distances 30 and 50 km and depths 0 and 30 km. Figure 3 shows the snap shots of wavefield in the vertical array.

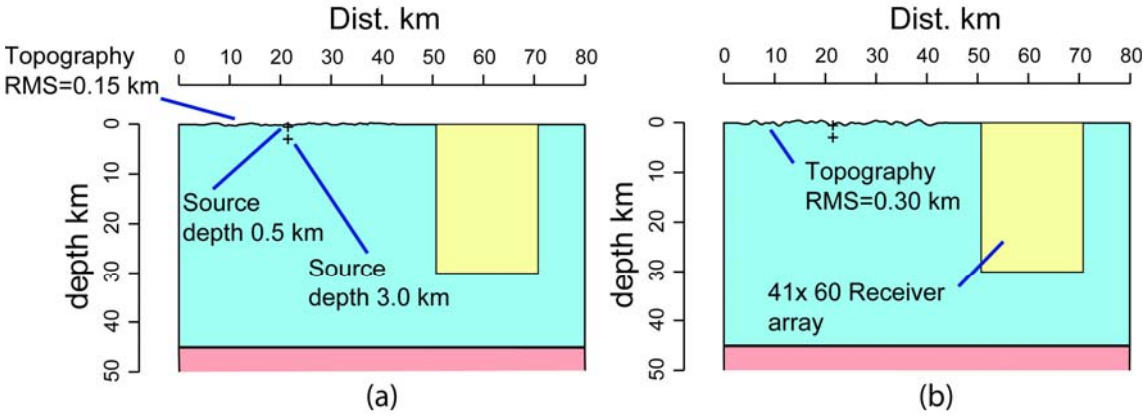

Figure 2. Cartoon showing the boundary element calculations and slowness analysis. Details given in the text.

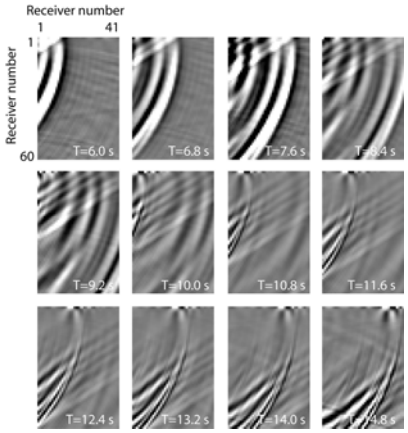

Figure 3. Wavefield snapshots from the vertical receiver array. Each time frame is independently normalized.

The synthetic seismograms are analyzed using the slowness analysis method (Xie et al. 2005a) to demonstrate how the energy partitioning is affected by the free surface fluctuations and the source depths. Illustrated in Figure 4 is the energy distribution in the horizontal-slowness and depth domain for different free surfaces and source depths. The red vertical lines indicate the upper mantle *S*-wave slowness. To the left of these lines, the waves have incidence angles steeper than the critical angle on the Moho and the energy will leak to the upper mantle through multiple reflections. To the right of these lines, total reflection will keep the energy in the crustal wave guide to contribute to the *Lg*-wave. In Figure 4, row (a) is for a flat free surface and a deeper explosion source. As expected, this configuration generates neither noticeable trapped energy nor clear *Rg*-wave. Row (b) is for a flat free surface and a shallow explosion source. The trapped energy is from *S**-wave. *Rg*-energy can be seen at very shallow depth for the shallow source. Row (c) is for a deeper explosion source and a free surface with 150 m rms fluctuation. Comparing with row (a), the existence of surface fluctuation generates considerable trapped energy from free surface scattering. Although the source is located at a depth of 3.0 km, the *Rg* energy can now be seen at shallow depth. This enhanced *Rg*-wave comes from the free surface scattering, which can be treated as shallow secondary sources. In rows (d) to (f), with shallower source or larger rms free surface fluctuations, a lot of trapped energy can be generated from the interaction between an explosion source and topographic fluctuations.

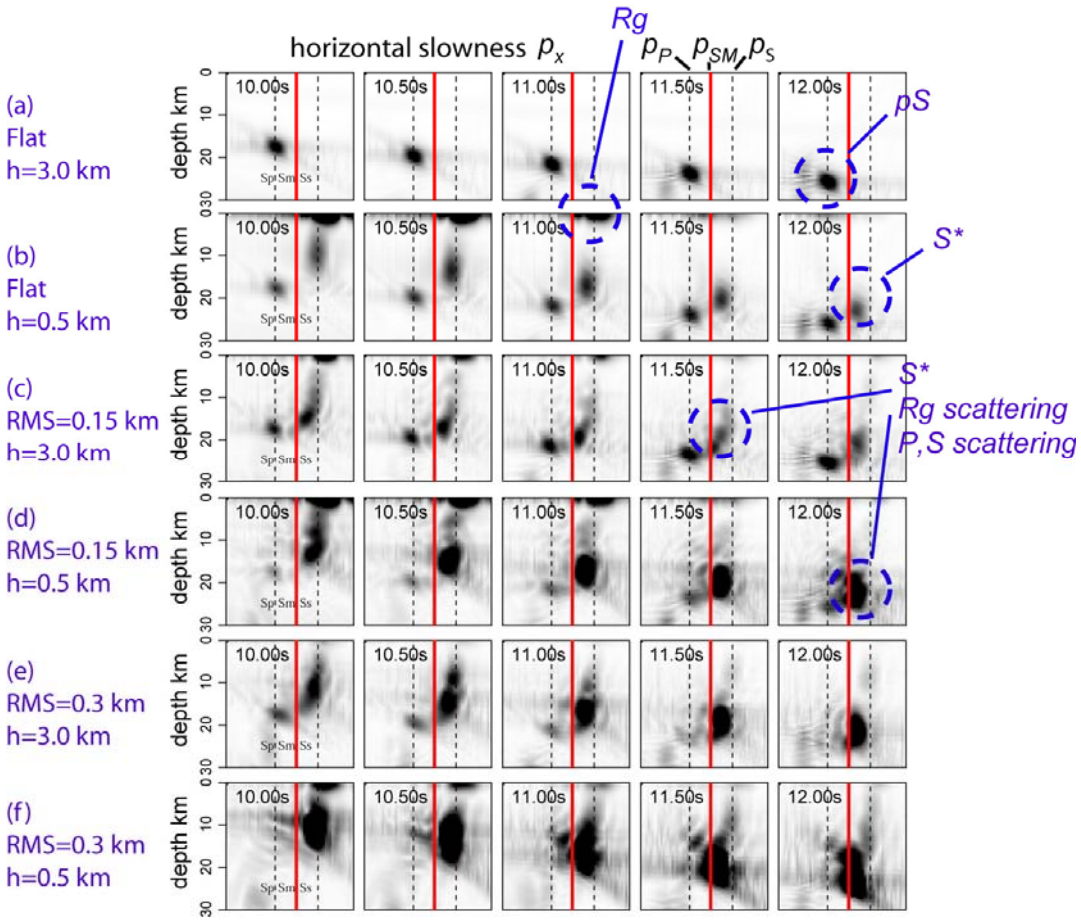

Figure 4. Slowness analysis for models with different source depths and free surface parameters. In each small panel, the horizontal coordinate is horizontal slowness and the vertical coordinate is depth. The red vertical lines indicate the upper mantle *S*-wave slowness which separates energy that leaks out of the waveguide (to the left) from energy trapped in the wave guide (to the right) that forms *Lg*.

The Effect of Surface Scattering on Energy Partitioning

We can symbolically write the near-source energy partitioning process for an explosion source as

$$E^K(p,f) = S(f)R^K(p,f), \tag{4}$$

where $E^K(p,f)$ is the near-source energy partitioned to the type *K* wave (*K* can be *P*, *S*, *Lg* , *Rg* or other wave types), p is the slowness, f is the frequency, and $S(f)$ is the spectrum of an isotropic explosion source. The $R^K(p,f)$ is the response of the near source structure to excite type *K* wave and can be expressed as

$$R^K(p,f) = R_F^K(p,f) + \sum_J R_F^J(p,f)T^{J\to K}(p,f), \tag{5}$$

where $R_F^K(p,f)$ is the response of a flat layered earth model and $T^{J\to K}(p,f)$ is the energy transfer function due to secondary effects such as near-source scattering or spall. In this study, we focus on the contribution from the surface scattering. The response function R_F^K partitions the source energy into different phases. The transfer function $T^{J\to K}$ provides the *J*-to-*K* coupling, which further modifies the partitioning by moving energy from one phase to another. The combined effect of R_F^K and $T^{J\to K}$ forms R^K, which partitions the energy radiated from an isotropic source into the *K*-wave energy distributed in slowness and frequency domains and this energy will later develop into different regional phases at remote distances. We allow $T^{J\to K}$ to take either positive or negative values. For example, if *J* type wave loses energy due to scattering, then $T^{J\to J}$ could be negative. Investigating these response and transfer functions provides a way to estimate the underlying process of energy partitioning. Due to the complex mechanisms involved, the actual near-source energy partitioning can be highly complex. Factors such as the source depth, local layered structure, attenuation, random velocity perturbations and free surface fluctuations all affect the partitioning. These effects often apply to the partitioning in a coupled way and the entire process may not necessarily be linear or simply separated. We will use numerical modeling to simulate the complex partitioning process and use slowness analysis to calculate these response functions. The above symbolic equations can provide us with a basic relationship to understand this process. The partitioning process relates to the space and time variables as well (Xie et al., 2005). We apply proper space and time windows to separate different phases for analysis. For simplicity, we omit the discussions on these variables.

Rg-to-*Lg* Coupling Due to Scattering from a Rugged Free Surface

To demonstrate the *Rg*-wave scattering on a rugged free surface, we calculate synthetic seismograms for the two-layer velocity model listed in Table 1. The source depth is 0.5 km. The random surface fluctuation is located between epicentral distances 5 and 25 km. It has a correlation length of 0.5 km and rms values vary between 0.0 and 0.4 km. The results of slowness analysis are shown in Figure 5 with different rows for models with different rms fluctuations. The *Rg* energy is located at depths less than 3 km and with a slowness similar to the *S*-wave. In row (a) with rms = 0, the *Rg*-wave is generated by the explosion source and a flat earth model. It arrives at the receiver array between 12 and 15 s and is labeled as "direct *Rg*-wave." The existence of rough free surface can cause scattering of different waves and redistribute their energy. As shallow secondary sources, these scattering interactions generate *Rg*-waves. In rows (b) to (d), there are early scattered *Rg*-waves between 10 and 12 s. They arrive earlier than the direct *Rg* because part of their wave path travels with faster body wave speed. We label this as "scattered *Rg*-wave." The amplitudes of *Rg*-waves depend on the same rms fluctuations that excite the scattered *Rg* but the roughness attenuates both direct and scattered *Rg*. The scattered energy may go to body waves as well. In row (e), due to strong scattering from a very rugged free surface, both direct and scattered *Rg*-waves are very weak.

Table 1. Two-layer velocity model

Bottom of layer (km)	V_P (km/s)	V_S (km/s)	ρ (g/cm^3)
45	6.5	3.6	2.9
infinity	8.0	4.5	3.3

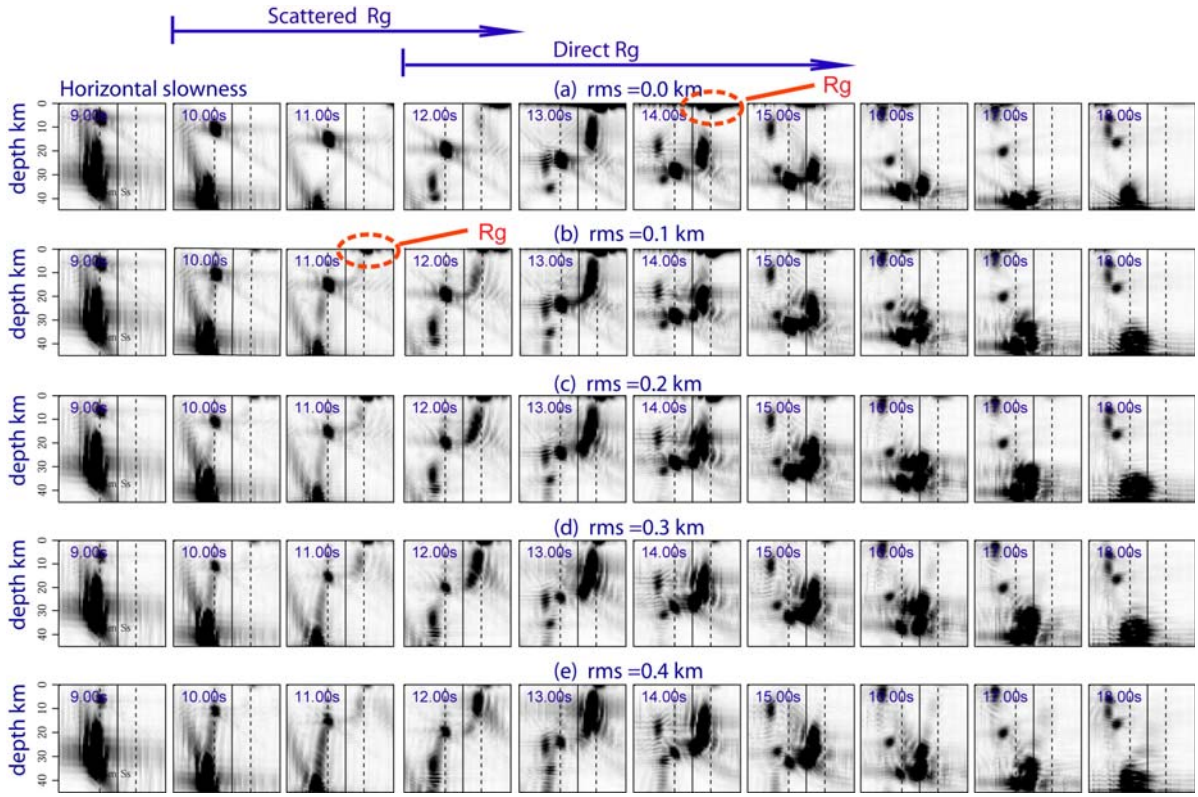

Figure 5. The slowness analysis for models with different rms topographic fluctuations. In each time frame the horizontal coordinate is the horizontal slowness and vertical coordinate is the depth. The *Rg* energy is located near the surface, with a slowness similar to the S-wave. Source depth is 0.5 km.

Applying proper frequency, slowness, time, and space windows to the slowness analysis result shown in Figure 5, we can separate the energy and estimate the excitation of different phases (Xie et al., 2005). For this purpose, we first calculate synthetic seismograms for a three-layer velocity model listed in Table 2. We use a source depth of 0.5 km. The random surface fluctuation is located above the source and extended in both directions for 20 km. The correlation length is 0.5 km and rms values vary between 0.0 and 0.4 km. A series of band pass filters are used to obtain responses between 0.75 and 4.0 Hz. In Figure 6, the top row illustrates the near-source responses of (a) direct *Rg*, (b) scattered *Rg* and (c) *Lg* as functions of frequency and rms surface fluctuations. For response function R^{Rg_direct}, the energy is mainly located at low frequencies and decreases with the increasing rms values. Note that the histograms labeled with rms = 0 indicate the response of a flat earth model.

Table 2. Three-layer velocity model

Bottom of layer (km)	V_P (km/s)	V_S (km/s)	ρ (g/cm^3)
10	5.6	3.2	2.7
45	6.5	3.8	2.9
Infinity	8.0	4.5	3.3

The contribution of the surface scattering can be calculated by subtracting the flat earth response from the total response (see Equation (5). The negative values of the differences shown in Figure 6 (d) indicate the energy loss of direct *Rg* due to the scattering attenuation, which is strong for larger rms values. The response of scattering *Rg* in Figure 6 (b) increases with increasing rms up to a moderate rms value, then decreases with further increasing rms. This suggests that small to moderate topographic fluctuation can excite secondary *Rg*-wave, but a very bumpy free surface will prevent the formation and propagation of *Rg*-waves. Because the time window of the direct *Rg* has some overlap with the scattered *Rg*, there is some energy in the scattered *Rg* window even for a flat earth model.

By subtracting this energy, we can obtain the pure scattering contribution, which is shown in Figure 6 (e). We see that this response is comprised of both low and high frequency contributions. It is possible that the former mainly comes from the *Rg*-to-*Rg* scattering and the later comes from body wave to surface wave scattering.

Shown in Figures 6 (c) and (f) are *Lg*-wave response R^{Lg} and separated scattering contribution $R^{Lg} - R_F^{Lg}$. The contribution of scattering to the *Lg*-wave is proportional to the rms values. Again, the contribution includes high frequency content which likely comes from the scattering of body waves to *Lg*, and low frequency content which mainly comes from *Rg*-to-*Lg* scattering. However, the low frequency content cannot be fully explained with the *Rg* energy loss. Although the low frequency spectrum of $R^{Lg} - R_F^{Lg}$ almost mirrors the shape of the $R^{Rg\_direct} - R_F^{Rg\_direct}$ spectrum, *Rg*-to-*Lg* coupling does not provide quite enough energy to *Lg*—this can be recognized by comparing the scales of (d) and (f). A possible explanation is that the additional low frequency *Lg* energy is provided by the body waves as well. A broadband body wave may excite low frequency S-waves if the surface scattering serves as shallow secondary sources. For example, a mechanism similar to the generation of *S** can provide a frequency dependent transfer function $T^{body \to Lg}$ in Equation (5). To verify this, additional study is required.

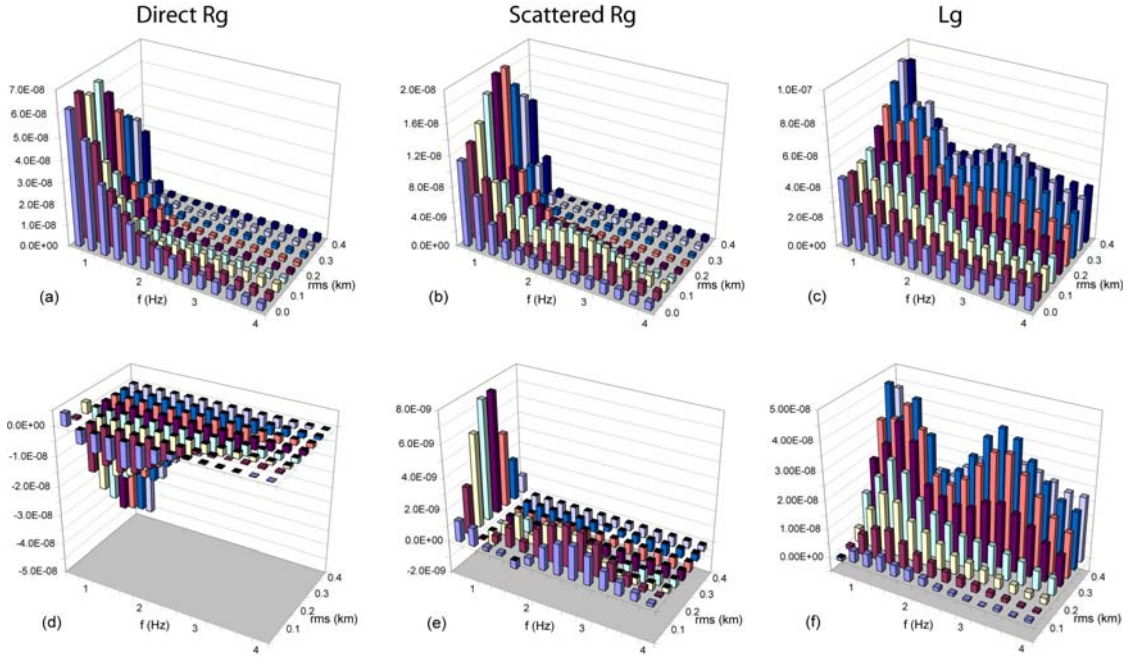

Figure 6. Top row: the near source responses of direct *Rg*, scattered *Rg* and the *Lg*-waves as functions of frequency and rms fluctuations, with (a) R^{Rg_direct}, (b) R^{Rg_scatt} and (c) R^{Lg}. Bottom row: the contributions of surface scattering to these responses, with (d) $R^{Rg\_direct} - R_F^{Rg\_direct}$, (e) $R^{Rg\_scatt} - R_F^{Rg\_scatt}$ and (f) $R^{Lg} - R_F^{Lg}$.

The Effect of Attenuation on the Energy Partitioning

Scattering from topographic fluctuations occurs within the topmost crust, which is usually a low *Q* layer. This attenuation will strongly affect the scattering and energy partitioning of an explosion source. To test the effect of attenuation, we introduce intrinsic attenuation in the boundary element calculation. We use the same source parameters, free surface parameters, and velocity model as used in Figure 6 except replacing the infinite *Q* in the top 10 km with $Q_P = 100$ and $Q_S = 50$. The results are shown in Figure 7. Comparing Figure 7 with Figure 6, two prominent features can be identified. First, compared to the purely elastic case, there is considerable energy loss in the model with intrinsic attenuation. For example, the maximum energy level drops 40% for direct *Rg*-wave, 70% for scattered *Rg*-wave, and 40% for *Lg*-wave. Second, the short period waves undergo more attenuation than long period waves. This is especially true for the scattered *Rg*-wave and the *Lg*-wave. By using rather low *Q* values in this calculation, this should give a maximum effect of the attenuation.

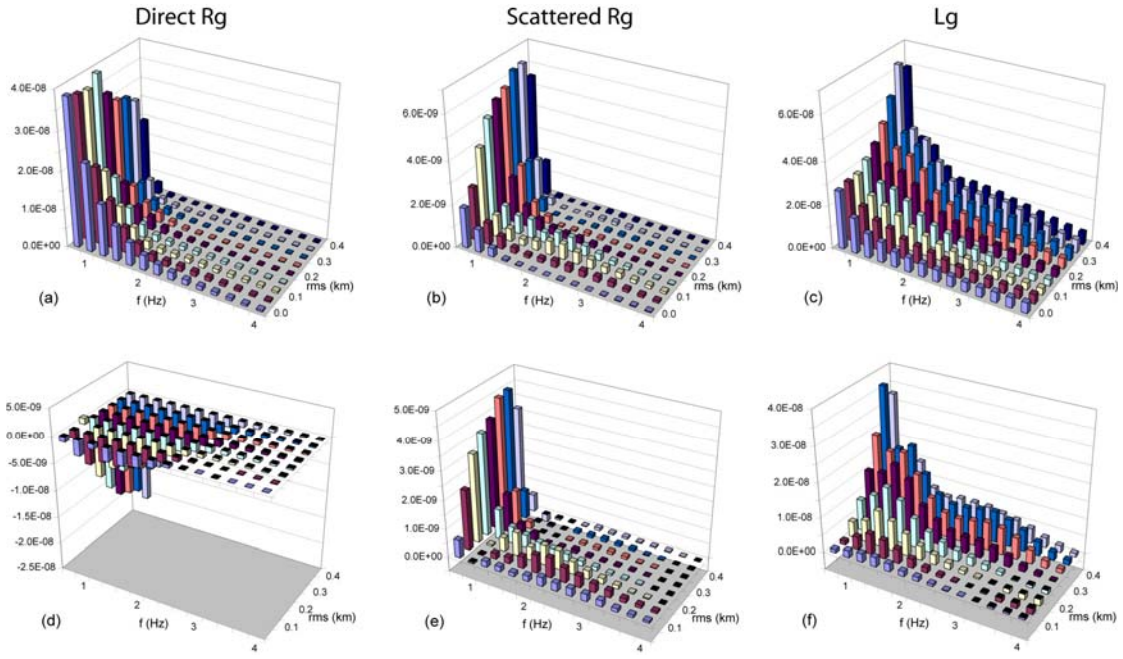

Figure 7. Similar to that shown in Figure 6, except low *Q* values are used in the top layer.

CONCLUSIONS AND RECOMMENDATIONS

We used the 2D *P-SV* boundary-element simulation and slowness analysis method to investigate the effect of topographic scattering on the near-source energy partitioning. Topographic models with different rms fluctuations and correlation lengths and different source depths and attenuation were investigated using numerical simulations. The result revealed that the surface scattering has strong effect on *Rg*-waves. The scattering process can excite the *Rg*-wave for a moderately rugged topography but prevent the formation of *Rg*-wave if the surface is becoming too rugged. The free surface scattering can increase the *Lg*-wave energy. It is possible that both *Rg* and body waves contribute to the *Lg*-wave through surface scattering. The effect of intrinsic attenuation on the energy partitioning was also studied.

The numerical simulation and slowness analysis accomplished in this report are 2D. We did not consider the energy partitioned to the *SH* component. In addition, in many cases, the effect of the 2D scattering may not be exactly the same as the 3D scattering. Expansion of the analysis to full 3D models should be pursued. Consideration of the P/S spectral behavior is also planned for future analysis.

ACKNOWLEDGEMENT

The authors wish to thank Dr. Zengxi Ge for many discussions and kindly providing the boundary element code.

REFERENCES

Aki, K. and Richards, P. G. (1980). *Quantitative Seismology. Theory and Methods*. San Francisco: W.H. Freeman.

Bonner, J. B., H. J. Patton, A. C. Rosca, H. Hooper, J. Orrey, M. Leidig, and I. Gupta (2003). Aspects of Rg and Lg generation from the Shagan depth of burial explosions, in *Proceedings of the 25th Seismic Research Review—Nuclear Explosion Monitoring: Building the Knowledge Base*, LA-UR-03-6029, Vol. 2, pp. 384–394.

Bottone, S., M. D. Fisk, and G. D. McCartor (2002). Regional seismic event characterization using a Bayesian formulation of simple kriging, *Bull. Seism. Soc. Am*. 92: 2,277–2,296.

Fan, G. W. and T. Lay (1998a). Statistical analysis of irregular waveguide influences on regional seismic discriminants in China, *Bull. Seism. Soc. Am*. 88: 74–88.

Fan, G. W. and T. Lay (1998b). Regionalized versus single-station wave-guide effects on seismic discriminants in western China, *Bull. Seism. Soc. Am*. 88: 1,260–1,274.

Fan, G. W. and T. Lay (1998c). Statistical analysis of irregular waveguide influences on regional seismic discriminants in China: Additional results for Pn/Sn, Pn/Lg and Pg/Sn, *Bull. Seism. Soc. Am*. 88: 1,504–1,510.

Fisk, M. D., H. L. Gray, and G. D. McCartor (1996). Regional discrimination without transporting thresholds, *Bull. Seism. Soc. Am*. 86: 1,545–1,558.

Fisk, M. D. (2006). Source spectral modeling of regional *P*/*S* discriminants at nuclear test sites in China and the former Soviet Union, *Bull. Seism. Soc. Am*. (in press).

Ge, Z., L. Y. Fu, and R. S. Wu (2005). P-SV Wavefield connection technique for regional wave propagation simulation, *Bull. Seism. Soc. Am.* 95: 1,375–1,386.

Gupta, I. N., W. Chan, and R. Wagner (1992). A comparison of regional phases from underground nuclear explosions at East Kazakh and Nevada test sites, *Bull. Seism. Soc, Am*. 82: 352–382.

Gupta, I. N., T. Zhang, and R. A. Wagner (1997). Low-frequency Lg from NTS and Kazakh nuclear explosions: Observations and interpretations, *Bull. Seism. Soc. Am*. 87: 1,115–1,125.

Gupta, I. N., W. W. Chan, and R. A. Wagner (2005). Regional source discrimination of small events based on the use of Lg wavetrain, *Bull. Seism. Soc. Am*. 95: 341–346.

Hartse, H. E., S. R. Taylor, W. S. Phillips, and G. E., Randall (1997). A preliminary study of regional seismic discrimination in central Asia with emphasis on western China, *Bull. Seism. Soc. Am*. 87: 551–568.

Kim, W. Y., V. Aharonian, A. L. Lerner-Lam, and P. G. Richards (1997). Discrimination of earthquakes and explosions in southern Russia using regional high-frequency three-component data from IRIS/JSP Caucasus Network, *Bull. Seism. Soc. Am*. 87: 569–588.

Kim, W. Y., D. W. Simpson, and P. G. Richards (1993). Discrimination of earthquakes and explosions in the eastern United States using regional high-frequency data, *Geophys. Res. Lett*. 20: 1,507–1,510.

McLaughlin, K. L. and R. S. Jih (1988). Scattering from near-source topography: Teleseismic observations and numerical simulations, *Bull. Seism. Soc. Am.* 78: 1,399–1,414.

Myers, S. C., J. L. Wagoner, S. C. Larsen, A. Rodgers, K. Mayeda, K. D. Smith, and W. R. Walter (2003). Simulation of regional explosion S-phases (SIRES) project, in *Proceedings of the 25th Seismic Research Review—Nuclear Explosion Monitoring: Building the Knowledge Base*, LA-UR-03-6029, Vol. 1, pp. 117–124.

Myers, S. C., J. Wagoner, L. Preston, K. Smith, and S. Larsen (2005). The effect of realistic geologic heterogeneity on local and regional P/S amplitude ratios based on numerical simulations, in *Proceedings of the 27th Seismic Research Review: Ground-Based Nuclear Explosion Monitoring Technologies*, LA-UR-05-6407, Vol. 1, pp. 123–132.

Nuttli, O. W. (1986). Yield estimates of Nevada Test Site explosions obtained from Lg waves, *J. Geophys. Res*. 91: 2,137–2,151.

Patton, H. J. (2001). Regional magnitude scaling, transportability, and Ms:mb discrimination at small magnitudes, *Pageoph*, 158: 1,951–2,015.

Patton, H. J. and S. R. Taylor (1995). Analysis of Lg spectral ratios from NTS explosions: Implications for the source mechanisms of spall and the generation of Lg waves, *Bull. Seism. Soc. Am*. 85: 220–236.

Stevens, J. L., G. E. Baker, H. Xu, T. J. Bennett, N. Rimer, and S. M. Day (2003). The physical basis of Lg generation by explosion sources, in *Proceedings of the 25th Seismic Research Review—Nuclear Explosion Monitoring: Building the Knowledge Base*, LA-UR-03-6029, Vol. 2, pp. 456–465.

Taylor, S. R. (1996). Analysis of high frequency Pn/Lg ratios from NTS explosions and western U.S. earthquakes, *Bull. Seism. Soc. Am*. 86: 1,042–1,053.

Taylor, S. R., M. D. Denny, E. S. Vergino, and R. E. Glaser (1989). Regional discrimination between NTS explosions and western U.S. earthquakes, *Bull. Seism. Soc. Am*. 79: 1,142–1,176.

Taylor, S. R. and H. E. Hartse (1997). An evaluation of generalized likelihood ratio outlier detection to identification of seismic events in Western China, *Bull. Seism. Soc. Am*. 87: 824–831.

Walter, W. R., K. M. Mayeda, and H. Patton (1995). Phase and spectral ratio discrimination between NTS earthquakes and explosions—Part I: Empirical observations, *Bull. Seism. Soc. Am.* 85: 1,050–1,067.

Wu, R. S., S. Jin, and X. B. Xie (2000a). Seismic wave propagation and scattering in heterogeneous crustal waveguides using screen propagators: I SH waves, *Bull. Seism. Soc. Am*. 90: 401–413.

Wu, R. S., S. Jin, and X. B. Xie (2000b). Energy partition and attenuation of Lg waves by numerical simulations using screen propagators, *Phys. Earth and Planet. Inter*. 120: 227–243.

Wu, R. S., X. B. Xie, Z. Ge, X. Wu, and T. Lay (2003). Quantifying source excitation and path effects for high-frequency regional waves, in *Proceedings of the 25th Seismic Research Review—Nuclear Explosion Monitoring: Building the Knowledge Base*, LA-UR-03-6029, Vol. 1, pp. 172–181.

Xie, J. (2002). Source scaling of Pn and Lg spectra and their ratios from explosions in central Asia: Implications for the identification of small seismic events at regional distances, *J. Geophys. Res*. 107: B7, 10.1029/2001JB000509.

Xie, X. B. and T. Lay (1994). The excitation of Lg waves by explosions: A finite-difference investigation, *Bull. Seism. Soc. Am*. 84: 324–342.

Xie, X. B., Z. Ge, and T. Lay (2005a). Investigating explosion source energy partitioning and Lg-wave excitation using a finite-Difference plus slowness analysis method, *Bull. Seism. Soc. Am*. 95: 2,412–2,427.

Xie, X. B., T. Lay, and R. S. Wu (2005b). Near source energy partitioning for regional waves in 2d and 3d models, contributions of S*-to-Lg and P-to-Lg scattering, in *Proceedings of the 27th Seismic Research Review: Ground-Based Nuclear Explosion Monitoring Technologies*, LA-UR-05-6407, Vol. 1, pp. 249–258.